Analysis of Filter Tuning Techniques for Sequential Orbit Determination*

T. Lee, C. Yee, and D. Oza
Computer Sciences Corporation
Lanham-Seabrook, Maryland, USA 20706

Abstract

This paper examines filter tuning techniques for a sequential orbit determination (OD) covariance analysis. Recently, there has been a renewed interest in sequential OD, primarily due to the successful flight qualification of the Tracking and Data Relay Satellite System (TDRSS) Onboard Navigation System (TONS) using Doppler data extracted onboard the Extreme Ultraviolet Explorer (EUVE) spacecraft. TONS computes highly accurate orbit solutions onboard the spacecraft in realtime using a sequential filter. As the result of the successful TONS-EUVE flight qualification experiment, the Earth Observing System (EOS) AM-1 Project has selected TONS as the prime navigation system. In addition, sequential OD methods can be used successfully for ground OD. Whether data are processed onboard or on the ground, a sequential OD procedure is generally favored over a batch technique when a realtime automated OD system is desired.

Recently, OD covariance analyses were performed for the TONS-EUVE and TONS-EOS missions using the sequential processing options of the Orbit Determination Error Analysis System (ODEAS). ODEAS is the primary covariance analysis system used by the Goddard Space Flight Center (GSFC) Flight Dynamics Division (FDD). The results of these analyses revealed a high sensitivity of the OD solutions to the state process noise filter tuning parameters. The covariance analysis results show that the state estimate error contributions from measurement-related error sources, especially those due to the random noise and satellite-to-satellite ionospheric refraction correction errors, increase rapidly as the state process noise increases. These results prompted an in-depth investigation of the role of the filter tuning parameters in sequential OD covariance analysis.

This paper analyzes how the spacecraft state estimate errors due to dynamic and measurement-related error sources are affected by the process noise level used. This information is then used to establish guidelines for determining optimal filter tuning parameters in a given sequential OD scenario for both covariance analysis and actual OD. Comparisons are also made with corresponding definitive OD results available from the TONS-EUVE analysis.

1. Introduction

This paper presents the results of a study to examine the sensitivity of sequential orbit determination (OD) errors to the filter tuning parameters. The results are obtained primarily from covariance analyses performed to assess the navigation performance of the Tracking and Data Relay Satellite (TDRS) System (TDRSS) Onboard Navigation System (TONS) for two spacecraft missions—the Extreme Ultraviolet Explorer (EUVE) and the Earth Observing System (EOS). TONS is a sequential OD system based on the extended Kalman filter. It is capable of computing highly accurate orbit solutions onboard the spacecraft in realtime and processing TDRSS forward-link one-way Doppler measurements. The feasibility of the TONS navigation method was successfully demonstrated on the flight qualification experiment performed in conjunction with the EUVE mission (Reference 1). As a result of this success, the EOS Project has selected TONS as the prime navigation system for the EOS AM-1 mission.

A sequential OD system using a Kalman filter is normally tuned to prevent it from diverging. Filter divergence can occur when the terms in the covariance matrix approach zero, which in turn causes the computed Kalman gain to approach zero. Since the Kalman gain determines how much emphasis to place on the measurements in updating the filtered state, the filter will ignore any new measurement as the Kalman gain approaches zero, resulting in filter divergence. One way of preventing the filter from diverging is to add a certain level of process noise to the system model to account for the unmodeled error contributions. The addition of process noise prevents the covariance matrix terms from approaching zero, thereby preventing

* This work was supported by the National Aeronautics and Space Administration (NASA)/Goddard Space Flight Center (GSFC), Greenbelt, Maryland, under Contract NAS 5-31500.

the Kalman gain from approaching zero. The choice of the appropriate level of process noise is largely heuristic and depends to a large extent on what is known about the unmodeled state parameters. More detailed information about filter tuning can be found in Reference 2. Generally, the larger the process noise levels added to the covariance matrix, the larger the Kalman gain will become, thus placing more emphasis on the measurement information than on the dynamic state model in updating the filtered state. One consequence of this approach is that, as the applied process noise level increases, the contribution from any measurement-related error is likely to be magnified while the contribution from the dynamic error sources is likely to decrease. The choice of optimum filter tuning parameters therefore involves selecting optimum process noise levels in such a way that the combined contribution of the dynamic and measurement-related error sources to the OD errors is minimized.

The covariance analysis results are obtained using the Orbit Determination Error Analysis System (ODEAS) (Reference 3). ODEAS is a general-purpose linear error analysis tool used at the Goddard Space Flight Center (GSFC) Flight Dynamic Division (FDD) to support various missions. On the basis of a tracking scenario and the expected accuracies of the orbital dynamic models and measurement process, ODEAS provides the magnitudes and characteristics of the errors that can be expected in an OD process. In this study, such covariance analysis results are used to identify those error sources that are most sensitive to the process noise level variation and to illustrate how the optimum OD solutions are achieved by controlling the process noise level within the ODEAS framework.

Section 2 of this paper describes the analysis methods used in this study and details the results obtained; Section 3 gives a summary of the study and summarizes the conclusions.

2. Analysis Methods and Results

Covariance analyses were performed for the EUVE and EOS PM-1 spacecraft. In both cases, sequential error analysis simulations were performed by processing 2 days worth of tracking data. The EUVE spacecraft is in a near-circular orbit at a nominal altitude of 520 kilometers and an inclination of 28.5 degrees. The tracking data distribution used for the EUVE study is taken from the actual tracking data around January 17, 1993. The tracking data consisted of 23 tracking passes of one-way forward-link TDRSS Doppler data with pass lengths ranging from 2 to 40 minutes distributed over the 2-day timespan. The EOS PM-1 spacecraft will be in a near-circular frozen orbit at a nominal altitude of 705 kilometers, with an inclination of 98.2 degrees. The tracking data consist of 20 minutes of one-way forward-link TDRSS Doppler data per EOS orbit, which amounts to 29 tracking passes during the 2-day timespan. The EOS PM-1 spacecraft was selected for study rather than EOS AM-1 because previous error analysis results (Reference 4) indicated that the OD error contributions from the ionospheric refraction effects were found to be larger for EOS PM-1 than for EOS AM-1.

Two types of error analysis simulations were performed. In the first case, the orbital state of the TDRSS-user spacecraft (EUVE or EOS) is estimated together with the frequency bias of the ultrastable oscillator (USO) used for onboard frequency reference and the atmospheric drag coefficient. In the second case, the drag coefficient is treated as a considered error source instead of being estimated.

Throughout this study, the sequential filter was tuned using a process noise algorithm based on a linear variance growth model. In this model the process noise variance is assumed to grow linearly with time elapsed between measurements (Reference 3). The process noise computed is added to the propagated error covariance, which is used in computing the Kalman gain matrix. Brief descriptions of the ODEAS gain matrix computation and the time and measurement update algorithm for the covariance matrices are presented below. Using the notations of Reference 3, the time-updated covariance matrix, $P(t_i-)$, and the measurement updated covariance matrix, $P(t_i)$, at a measurement time t_i, are given by

$$P(t_i-) = \phi(t_i, t_{i-1})\, P(t_{i-1})\, \phi^T(t_i, t_{i-1}) + Q_i \tag{1}$$

$$P(t_i) = (I - K_i \Omega_i)\, P(t_i-)(I - K_i \Omega_i)^T + K_i R K_i^T \tag{2}$$

where $\phi(t_i, t_{i-1})$ denotes the state transition function and K_i the Kalman gain matrix. The gain matrix, K_i, is defined in terms of R, the measurement noise variance (MNV), Ω_i, the measurement partial derivative matrix, and $P(t_i-)$, the time updated covariance matrix, as follows:

$$K_i = P(t_i-)\Omega_i^T\left(R+\Omega_i P(t_i-)\Omega_i^T\right)^{-1} \tag{3}$$

The matrix Q_i on the right-hand side of Equation (1) represents the process noise. The ODEAS linear growth process noise model defines Q_i as follows:

$$Q_i \equiv D\cdot(t_i - t_{i-1}) \tag{4}$$

The quantity D in the above equation is a diagonal matrix with the variance growth rate of solve-for parameters as diagonal elements. For the nonorbital solve-for parameters such as the clock drift, an additional restriction is imposed such that the computed process noise level, Q_i, does not exceed the respective *a priori* variance. In the present study, D is assumed to be of a special form in which the only nonzero elements are those associated with the user spacecraft velocity components and the clock drift parameter. It is further assumed that the three velocity variance growth rates are the same: that is, a single variance growth rate parameter, designated here as Qdot, is assigned for all three velocity components. The characteristic behavior of the state estimate errors due to major error sources are investigated when the process noise level is varied by specifying different values for the velocity variance growth rate and the MNV parameters. In this paper, the name Qdot will be used to denote the velocity variance growth rate. The value of MNV is obtained by squaring the measurement noise standard deviation (MNSD) specified for the tracking measurements. The variance growth rates for the estimated clock drift (frequency bias) and the drag coefficient (when the drag is estimated) are not varied.

Given below is a description of the methods and results of the EUVE and EOS PM-1 studies, followed by a brief comparison of the EUVE and EOS filter tuning results and a description of the covariance analysis versus the actual OD results.

2.1 EUVE Study

The methods and results of the EUVE filter tuning analysis are presented below.

EUVE Methods

The major error sources included in the EUVE covariance analysis are summarized in Table 1. The measurement-related error sources included are the measurement noise specified by the MNSD, TDRS ephemeris errors, and satellite-to-satellite tracking (SST) ionospheric refraction errors. The major dynamic error sources included are the atmospheric drag and gravity errors. Orbital errors due to the gravity model uncertainties are computed using the Goddard Earth Model-T3 (GEM-T3) standard errors in the ODEAS uncorrelated error model approach (UEMA) (Reference 2). The EUVE results presented here are based on solutions in which the drag coefficient error is included as a considered error source.

Table 1. Major Error Sources Included in the EUVE Analysis

Error Sources	3σ Errors	Notes
Measurement noise	0.001meter/second and 0.01 meter/second	TDRS one-way range-rate measurements
TDRS ephemeris errors	5 meters, 30 meters, 40 meters in the radial, cross-track, and along-track (HCL) directions	For both TDRS-East and TDRS-West
Ionospheric refraction errors	100% of measurement delay	Bent ionospheric model
Drag coefficient error	30% (when considered)	Harrirs-Priester model with $F_{10.7} = 122 \times 10^{-22}$ watts/meter^3/hertz
Geopotential errors	GEM-T3 30 × 30 sigmas	ODEAS UEMA model

The sensitivities of the solution errors to the process noise level applied are studied with two groups of error analysis solutions, referred to as the Group A and Group B solutions and defined as follows:

- Group A solutions are obtained using an MNSD of 0.001 meter/second, while the Qdot value is varied from zero to 1.0×10^{-9} meter^3/second^2 (a total of six solutions obtained using six different Qdot values given by 0.0, 1.0×10^{-13}, 1.0×10^{-12}, 1.0×10^{-11}, 1.0×10^{-10}, and 1.0×10^{-9} meter^3/second^2).
- Group B solutions are obtained using an MNSD of 0.01 meter/second and the same set of Qdot values used for the Group A solutions. Note that the MNSD values used in Group B solutions are 10 times that of Group A solutions.

EUVE Results

The variation of the covariance analysis solutions with respect to the process noise levels may be better characterized in terms of their statistical properties. The root-mean-square (RMS) position errors and their standard deviations (SDs) are summarized in Table 2, together with their maximum and minimum values. The proportionality of the error magnitudes to the Qdot values used is clearly demonstrated in this table. This table also suggests two simple relations that hold between the Group A and Group B solutions. The first relation is that for solutions obtained without filter tuning, the RMS values and standard deviations are proportional to the MNSD values used (see the last column of Table 1). Note that the Group B results are 10 times the corresponding Group A results, which is the same ratio as the ratio of the MNSD values used for the two groups of solutions. This relation is expected because normally the orbital errors due to the random noise in the steady state period are almost entirely due to the measurement noise.

Table 2. Random Noise Contributions to EUVE Position Errors

Error Statistics	Velocity Filter Tuning Parameter (Qdot) (meter^2/sec^3)					
	1.0×10^{-9}	1.0×10^{-10}	1.0×10^{-11}	1.0×10^{-12}	1.0×10^{-13}	0.0
Group A Solution Statistics (meters) MNSD = 0.001 meter/second						
RMS	5.8936	3.6452	2.3136	1.2901	0.7462	0.4387
SD	3.9215	2.4453	1.5499	0.7336	0.2756	0.0719
Maximum	24.6185	14.8740	11.2404	5.2263	1.9792	0.6270
Minimum	1.5354	0.9985	0.5951	0.4437	0.3591	0.2841
Group B Solution Statistics (meters) MNSD = 0.01 meter/second						
RMS	23.1428	12.9020	7.4623	5.2429	4.5294	4.3873
SD	15.5054	7.3367	2.7562	1.0732	0.7302	0.7191
Maximum	112.4479	52.2718	19.7915	8.1712	6.2792	6.2699
Minimum	5.9508	4.4371	3.5907	3.2023	2.9438	2.8409

A close examination of Table 2 suggests a second relation between the Group A and Group B solutions obtained using finite Qdot values. This relation indicates that the orbital error statistics associated with a Group B solution are approximately 10 times those of the Group A solution that is obtained with a Qdot value that is 100 times smaller than the one used for the Group B solution. For example, the RMS and SD values of the Group B solution obtained using a Qdot value of 1.0×10^{-11} are 10 times those of the Group A solution obtained using a Qdot value of 1.0×10^{-13}. These two solutions can be characterized as having the same Qdot-to-MNV ratio. The MNV value is obtained by squaring the MNSD value. The Group A solutions used an MNV of 1.0×10^{-6} meter^2/second^2, whereas the Group B solutions used an MNV value of 1.0×10^{-4} meter^2/sec^2. This gives a Qdot-to-MNV ratio of 1.0×10^{-7} (in units of 1/second) in the case of the two sample solutions. The first relation described above can be considered as a special case of this second relation because the solutions obtained without filter tuning can be characterized as having a zero Qdot-to MNV ratio. Thus, Group B solutions can be obtained from Group A solutions obtained using the same Qdot-to-MNV ratios (by multiplying the latter with the ratio of the MNSD values used). This second relation is not as obvious as the first one, but it too can be verified using the ODEAS filter tuning algorithm described earlier.

The very structure of Equations (1) through (3) implies two things in the steady-state region:

- The matrix defined as the covariance matrix divided by MNV is determined by the Qdot-to-MNV ratio only.
- The Kalman gain matrix is determined only by the Qdot-to-MNV ratio as well.

Since the random noise conributions are derived from the covariance matrix, the results summarized in Table 2 are totally consistent with the first of these two asserions. The second property states that the gain matrix is entirely determined by the Qdot-to-MNV ratio only. Figure 2 verifies this assertion numerically. This figure shows the x-components of two gain matrices obtained using the same Qdot-to-MNV ratio in the steady-state region. The vertical axis represents the x-components of the gain matrices expressed in units of meters/(meters/second). Both gain matrices were obtained using a Qdot-to-MNV ratio of 1.0×10^{-6}. The x-components of the two gain matrices are seen to be almost identical. Since the error budgets due to systematic error sources are determined by the gain matrix only, this implies that all orbital error contributions from the measurement-related and dynamic error sources will be determined only by the Qdot-to-MNV ratio as well. As such an example of the dynamical error contributions, the EUVE position errors due to the atmospheric drag error are summarized in Table 3. Similar behavior is observed for position error contributions from the other systematic error sources considered.

The results summarized in Tables 2 and 3 show that, as the process level (or equivalently, the Qdot-to-MNV ratio) increases, the orbital errors due to the measurement-related error sources generally increase while those due to the dynamical error sources decrease. These features are expected from the theoretical considerations mentioned earlier. It should be noted that the SDs of these orbital errors have similar trends. The orbital errors due to the SST ionospheric refraction errors and those due to the atmospheric drag errors were found to be most sensitive to the process noise level changes. The gravity model uncertainty is usually one of the major dynamical error sources, contributing approximately 25 meters to the position errors for the EUVE OD solutions examined here. However, as discussed earlier, the orbital errors due to the gravity model uncertainties were found to be relatively insensitive to the Qdot-to-MNV ratio.

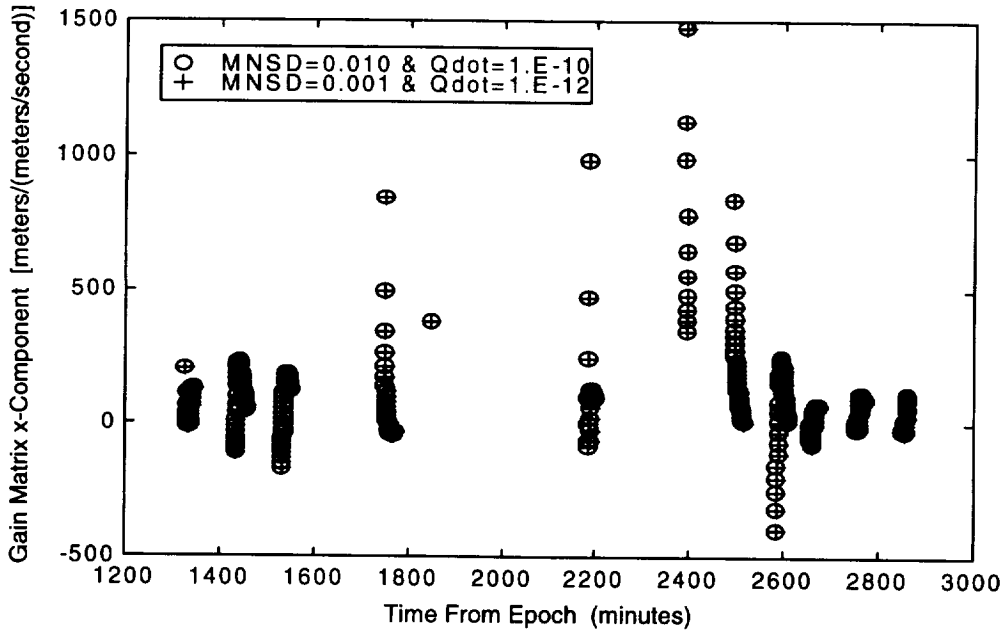

Figure 2. Behavior of x-Components of Gain Matrices

Table 3. Atmospheric Drag Error Contributions to EUVE Position Errors

Error Statistics	Velocity Filter Tuning Parameter (Qdot) (meter^2/second^3)					
	1.0×10^{-9}	1.0×10^{-10}	1.0×10^{-11}	1.0×10^{-12}	1.0×10^{-13}	0.0
Group A Solution Statistics (meters) MNSD = 0.001 meter/second						
RMS	1.2681	1.3643	1.9223	3.4975	6.5251	137.8619
SD	2.5499	2.8581	3.8017	4.7522	6.8147	67.5221
Maximum	21.6648	22.0163	27.8274	36.8109	45.1079	275.8270
Minimum	0.1824	0.0666	0.2418	0.6395	0.9928	20.1890
Group B Solution Statistics (meters) MNSD = 0.01 meter/second						
RMS	1.9223	3.4975	6.5251	12.6430	30.5039	137.8630
SD	3.8017	4.7522	6.8147	9.9910	15.9932	67.5224
Maximum	27.8273	36.8109	45.1079	52.7269	76.9703	275.8284
Minimum	0.2418	0.6395	0.9928	1.5085	9.6304	20.1892

The RMS position errors discussed above without the contribution from the gravity model uncertainty are summarized in Table 4. This table shows that Case 3 which uses the Qdot-to-MNV ratio of 1.0×10^{-8}, gives the optimum solution for both Group A and Group B solutions. The random noise contribution does not play a significant role in either group of solutions. The consider error contributions, especially those due to the SST ionospheric refraction and the drag model uncertainties, determine the optimum filter tuning parameters in the EUVE results presented here.

Table 4. EUVE RMS Position Errors Versus Qdot-to-MNV Ratio

Cases Studied		Group A Solutions (MNSD = 0.001 meter/second)			Group B Solutions (MNSD = 0.01 meter/second)		
Case No.	Qdot-to-MNV Ratio	Consider[a] Errors	Random Noise	Total	Consider[a] Errors	Random Noise	Total
1	0.0	156.2926	0.4387	156.2932	156.2937	4.3873	156.3552
2	1.0×10^{-9}	45.4391[b]	0.4529[b]	45.4413	45.4391	4.5295	45.6643
3	1.0×10^{-8}	34.5827[b]	0.5243[b]	34.5867	34.5827	5.2429	34.9779
4	1.0×10^{-7}	36.8580	0.7462	36.8655	36.8576	7.4623	37.6055
5	1.0×10^{-6}	63.8592	1.2901	63.8722	63.8540	12.9020	65.1444
6	1.0×10^{-5}	127.4191	2.3136	127.4401	127.4037	23.1428	129.4886
7	1.0×10^{-4}	203.2214	3.6452	203.2541	203.2214[c]	36.4523[c]	206.4647
8	1.0×10^{-3}	310.2432	5.8936	310.2992	310.2432[c]	58.9364[c]	315.7916

a: Consider columns: These columns include systematic error contributions from TDRS ephemeris errors, SST ionospheric refraction errors (100%), gravity errors, and the drag errors (30% of C_D). Consider contributions for Case 1 are mostly from the drag errors, and those for Case 8 are mostly from the SST ionospheric refraction errors.

b: These results are obtained from the corresponding Group B solutions.

c: These results are obtained from the corresponding Group A solutions.

To see the influence of the ionospheric refraction and drag errors in determining the optimum Qdot-to-MNV ratio, four series of solutions were constructed in which different magnitudes of the ionospheric refraction and drag errors were assumed. The total RMS position errors based on the Group B solutions are shown in Figure 3. The x-axis of the graph indicates the case number defined in the first column of Table 4. The solid curve represents the results given in the last column of Table 4.

The solution curves split into two groups at each end of the graph. The splits at the right-hand side of the graph are due to the different ionospheric refraction errors assumed, and those at the left-hand side of the graph are due to the different

amount of drag errors assumed. Note that high SST ionospheric refraction errors and low drag errors increase the optimum value of the Qdot-to-MNV ratio. The optimum value for the Qdot-to-MNV ratio remains at 1.0×10^{-8} (Case 3) for three of the solution series, and it changed to 1.0×10^{-7} (Case 4) for the solutions represented by the broken line, which were obtained assuming high drag errors (30 percent) and more moderate ionospheric refraction errors (50 percent). Given the error sources and their relative strengths, the optimum Qdot-to-MNV ratios lie somewhere between 1.0×10^{-7} and 1.0×10^{-9} (Cases 2, 3, and 4). Since different spacecraft missions will have different relative magnitudes of the measurement-related errors (especially the SST ionospheric refraction errors) and the dynamical errors (especially the drag errors), this range of optimum Qdot-to-MNV ratios will vary from spacecraft mission to spacecraft mission. It should also be noted that, in the case of the results presented above for EUVE, the range of the optimum values of the Qdot-to-MNV ratio may have been somewhat underestimated because the gravity error contributions are not included. Inclusion of the gravity error contributions will increase the optimum Qdot-to-MNV ratio, especially when the SST ionospheric refraction errors are small.

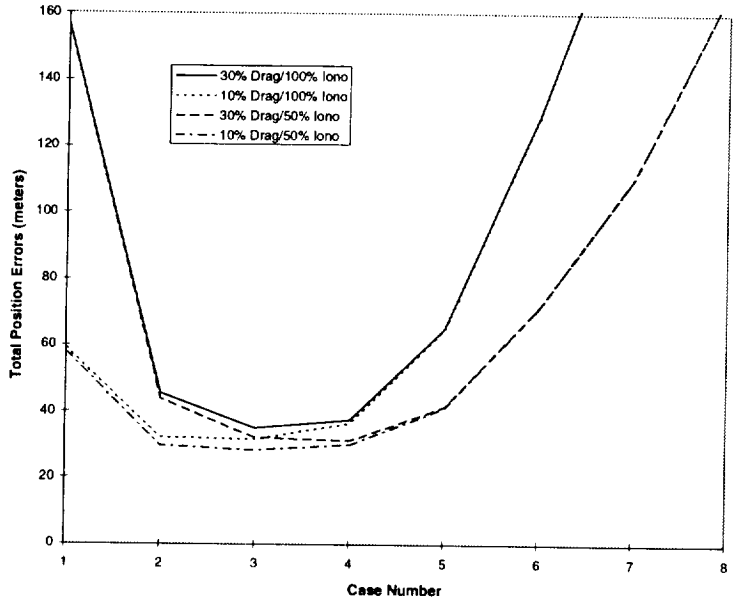

Note: Four series of solutions are shown in this graph. The case number (x-axis) indicates the Qdot-to-MNV ratio used as defined in Table 4. All four series of solutions were obtained using an MNSD of 0.01 and assuming different amounts of the atmospheric drag and ionospheric refraction errors on the SST links.

Figure 3. Influence of Drag and SST Ionospheric Refraction Errors on the Determination of Optimum Filter Tuning Parameters

When the drag coefficient is estimated, it practically eliminates the drag-related errors. Although solar flux uncertainties will still contribute to the drag error, the drag estimation process absorbs most of the solar flux errors, leaving only a small residual effect as the drag-related error contribution to the orbital error. This may be due to the limited nature of the ODEAS drag error modeling, which, for example, could not take the atmospheric effects associated with the geomagnetic storms into account. Assuming a 30-percent solar flux error, this residual solar flux uncertainty contributes less than 5 meters (3.5 meters RMS) to the orbital position errors. This drag contribution is reduced by using a finite Qdot-to-MNV ratio, but the effect is too small to counteract the sizable increase in the measurement-related error contributions, especially those due to the SST ionospheric refraction errors. Thus, it is not surprising to see that the minimum total position error was achieved with no filter tuning when the drag coefficient is estimated. This means that the optimum Qdot-to-MNV ratio for the EUVE OD scenario studied here will be smaller than the smallest finite ratio (1.0×10^{-9}) included in the study.

2.2 EOS PM-1 Study

The methods and results of the EOS PM-1 filter tuning analysis are presented below.

EOS PM-1 Methods

The major error sources included for the EOS PM-1 analysis are shown in Table 5. These error models are somewhat different from those used for the EUVE analysis. In particular, the TDRS ephemeris errors and the daily solar flux levels used for the EOS PM-1 analysis are much higher than than those used for the EUVE analysis. The EOS errror models were selected to simulate a different physical and operational environments.

Table 5. Major Error Sources Included in the EOS PM-1 Analysis

Error Sources	3σ Errors	Notes
Measurement noise	0.00118 meter/second	TDRS one-way range-rate measurements
TDRS ephemeris errors	66 meters, 60 meters, and 120 meters in the HCL directions	For both TDRS-East and TDRS-West
Ionospheric refraction errors	100% of measurement corrrection	Bent ionospheric model
Drag coefficient error	30% (when considered)	Harris-Priester model with $F_{10.7} = 250 \times 10^{-22}$ watts/meter^2/hertz
Geopotential errors	GEM-T3 30 × 30 sigmas	ODEAS UEMA model

Table 6 provides a description of two series of error analysis solutions. In the first series, designated as Series C, the EOS spacecraft state was estimated together with the USO frequency bias used for the onboard frequency reference. The atmospheric drag coefficient error was treated as a considered error source, together with the TDRS ephemeris uncertainties, gravitational potential uncertainties, and other standard error sources. The filter was tuned by applying process noise on the spacecraft velocity and the USO frequency bias. To assess how filter tuning affects the OD errors, various velocity process noise levels were applied in terms of velocity variance growth rates ranging from 5×10^{-15} meter^2/second^3 to 5×10^{-9} meter^2/second^3. This corresponds to Qdot-to-MNV ratios ranging from 5.0×10^{-9} to 5.0×10^{-3}. In all simulations, the USO frequency bias process noise level was set at a variance growth rate of 1.0×10^{-6} nanosecond^2/second^3.

Table 6. Two Series of Covariance Analysis Simulations

Simulation Case	Solve-for Parameters	Qdot-to-MNV Ratio	Velocity Variance Growth Rate for Filter Tuning
C1	EOS State, USO Bias	5×10^{-9}	5×10^{-15}
C2		5×10^{-7}	5×10^{-13}
C3		5×10^{-5}	5×10^{-11}
C4		5×10^{-3}	5×10^{-9}
D1	EOS state, USO bias, and drag coefficient	0.0	0.0
D2		5×10^{-9}	5×10^{-15}
D3		5×10^{-7}	5×10^{-13}
D4		5×10^{-5}	5×10^{-11}
D5		5×10^{-3}	5×10^{-9}

In the second series, designated as Series D, the EOS spacecraft state was estimated together with the USO frequency bias and the drag coefficient. Again, to assess the effects of filter tuning on the OD errors, various velocity process noise levels were employed with variance growth rates ranging from 0.0 (for no filter tuning) to 5×10^{-9} meter^2/second^3. This corresponds to Qdot-to-MNV ratios ranging from 0.0 to 5.0×10^{-3}. No process noise was applied to the drag coefficient or the USO frequency bias.

A daily $F_{10.7}$ solar flux level of 250×10^{-22} watts/meter^2/hertz was assumed for the Harris-Priester atmospheric density calculations throughout the analysis. Note that for Series C the drag coefficient was treated as a considered error source with an *a priori* uncertainty of 30 percent, and the effect of the daily solar flux uncertainty was not modeled. In Series D, the drag coefficient was solved for together with the EOS state, thereby eliminating the direct contribution of this error source on the OD error. However, to account for the residual effect of atmospheric-drag-related error contribution on the OD error, an *a priori* uncertainty of 30 percent in the daily solar flux was assumed. In all error analysis simulations, tracking schedules with favorable TDRSS tracking geometries were selected. A favorable TDRSS tracking geometry is realized by selecting tracking passes with high rates of change in the Doppler data during a tracking pass. This can be achieved when the orbit orientations of TDRS and EOS PM-1 are such that the angle between the TDRS vector and the EOS PM-1 orbit normal vector is close to 90 degrees. The maximum Doppler rate is achieved when this angle is 90 degrees.

EOS PM-1 Results

Table 7 summarizes the error analysis results obtained for simulation Series C. The results include the maximum and RMS position error contributions from various error sources after 1 day of tracking. The maximum position errors range from 66 meters to 604 meters (3σ), and the RMS position errors range from 32 meters to 378 meters (3σ), depending on the process noise levels used. The results show that the EOS total position error reaches a minimum for simulation C3, which uses a process noise level of 5.0×10^{-11} meter^2/second^3 (corresponding to a Qdot-to-MNV ratio of 5.0×10^{-5}). Major error sources include the ionospheric refraction from TDRS to EOS tracking links, the atmospheric drag, the TDRS ephemeris uncertainties, and the gravity potential uncertainties.

Table 7. RMS Position Error Contributions From Various Error Sources After 1 Day of Tracking

Statistical Quantity	Simulation Case	3σ Position Errors (meters)						
		Total	Drag	Gravity	TDRS Ephemeris	Ionospheric Effect via TDRS-5	Ionospheric Effect via TDRS-4	Noise
Maximum	C1*	603.96	603.52	21.18	18.59	12.67	10.34	1.71
	C2*	191.99	190.71	15.24	20.36	16.53	13.65	1.92
	C3**	66.09	40.35	16.08	29.12	58.56	21.36	3.22
	C4**	137.74	21.33	24.02	125.15	118.81	20.13	5.49
RMS	C1*	377.67	377.11	15.82	9.96	6.84	4.46	1.13
	C2*	133.00	131.67	11.50	10.17	8.79	5.54	1.34
	C3**	31.74	17.27	10.47	13.93	18.07	8.04	2.27
	C4**	52.49	8.26	11.09	41.69	26.81	8.84	3.64

* Filter does not stabilize within 2 days of tracking

** Filter stabilizes after 1 day of tracking

Again, as was observed with the EUVE results, Table 7 shows that as the process noise level increases the RMS position errors resulting from the dynamic error sources (such as gravity and atmospheric drag uncertainties) decrease, while those due to measurement-related error sources (such as ionospheric refraction, TDRS ephemeris uncertainties, and measurement noise) increase. In simulation C1, using a velocity process noise level of 5×10^{-15} meter^2/second^3, the atmospheric drag uncertainty was a major error source, causing the EOS position error to increase to 604 meters after 1 day of tracking. However, with an increased velocity process noise level of 5×10^{-11} meter^2/second^3, as in simulation C3, the contribution

from the atmospheric drag uncertainty was substantially reduced, causing the EOS position errors to stabilize at less than 50 meters (3σ) after about 1.5 days of tracking. However, in this case, the OD error contribution from SST ionospheric refraction was magnified, causing it to become one of the major error sources.

Table 8 summarizes the error analysis results obtained for simulation Series D. In this series, the atmospheric drag coefficient is estimated, not considered. The results include the maximum and RMS position error contributions from various error sources after 1 day of tracking. The maximum position errors range from 36 meters to 140 meters, and the RMS position errors range from 22 meters to 57 meters, depending on the filter-tuning approach used. The results show that the total position error reaches a minimum for simulation Case D2 (i.e., using a velocity variance growth rate of 5×10^{-15} meter^2/second^3, corresponding to a Qdot-to-MNV value of 5×10^{-9}). Major error sources include the gravity potential, the ionospheric refraction effect on the TDRS-5 to EOS tracking link, and the TDRS ephemeris uncertainties.

Table 8. Maximum and RMS Position Errors Contributed From Various Error Sources After 1 Day of Tracking

Statistical Quantity	Simulation Case	3σ Position Errors (meters)						
		Total	Gravity	Solar Flux	TDRS Ephemeris	Ionospherice Effect via TDRS-5	Ionospheric Effect via TDRS-4	Noise
Maximum	D1**	58.09	19.87	9.18	55.55	3.79	3.74	0.29
	D2**	34.48	17.35	11.96	23.08	22.45	17.27	2.45
	D3**	35.76	16.18	13.74	23.25	23.89	17.16	2.46
	D4**	65.64	16.81	13.99	30.85	61.20	20.64	3.28
	D5*	139.41	23.72	7.72	126.59	120.47	20.06	5.87
RMS	D1**	30.49	13.68	4.77	26.49	2.27	2.06	0.19
	D2**	21.61	12.75	5.31	10.43	11.26	7.35	1.64
	D3**	21.89	11.94	5.74	10.57	11.35	7.12	1.66
	D4**	27.29	10.67	6.28	14.53	18.38	7.87	2.35
	D5*	56.77	10.78	3.39	47.55	27.04	9.03	3.70

* Filter does not stabilize within 2 days of tracking

** Filter stabilizes after 1 day of tracking

Again, looking at the RMS values, the EOS position errors resulting from the dynamic error sources, such as the gravity potential, decrease as the process noise level increases. The reverse trend is true for measurement-related error sources, such as the ionospheric refraction. An exception is the EOS position error contribution from TDRS ephemeris uncertainties when filter tuning is not applied (simulation D1). The RMS position error contributed by this error parameter is found to be larger in simulation case D1, where no process noise is applied, than those obtained in cases D2, D3, or D4, where certain process noise levels are applied. The exact cause for the result obtained in case D1 is not known and will require additional analysis. The other simulation cases, D2 through D5, followed the expected trend.

In case D1, where no process noise is applied, the position error stabilizes at less than 60 meters after 1 day of tracking. With some amount of process noise (Case B2 with a process noise level of 5×10^{-15} meter^2/second^3), the position error further decreases to less than 40 meters. However, any further increase in process noise levels causes the EOS position error to increase once again. For Case D5, the EOS position error does not reach a steady-state condition within 2 days of tracking. This is due to the fact that by using a relatively large process noise level, the filter behavior is now controlled primarily by the information provided by each measurement rather than by the cumulative memory provided by the filtered state, causing the orbital error to fluctuate with measurement information.

The EOS PM-1 results summarized above demonstrate that the process noise applied for filter tuning can significantly affect the orbit determination error contributions from various error sources in different ways. It was shown that, in general, the EOS position errors resulting from dynamic error sources, such as gravity potential and atmospheric drag, decrease as the process noise level increases. The reverse trend was found to be true for measurement-related error sources, such as

ionospheric refraction and TDRS ephemeris uncertainty. These findings are consistent with the theoretically expected trend noted earlier.

For Series C, the maximum position errors ranged from 67 to 604 meters, and the corresponding RMS position errors ranged from 32 meters to 378 meters, depending on the filter-tuning approach used. Optimum filter tuning was achieved using a Qdot value of 5.0×10^{-11} meter^2/second^3 (corresponding to a Qdot-to-MNV ratio of 5.0×10^{-5}). Major error sources include ionospheric refraction from the TDRS-5 to EOS tracking link, atmospheric drag, solar flux, and TDRS ephemeris and gravity potential uncertainties. For Series D, the maximum position errors ranged from 36 meters to 140 meters, and the RMS position errors ranged from 22 meters to 57 meters, depending on the filter-tuning approach used. Optimum filter tuning was achieved using a Qdot value of 5.0×10^{-15} meter^2/second^3 (corresponding to a Qdot-to-MNV ratio of 5.0×10^{-9}). Optimum process noise levels were found to be smaller than those used in Series C because of the smaller dynamic error contributions in this series. Major error sources include gravity, ionospheric refraction effect on the TDRS-5 to EOS tracking link, and TDRS ephemeris uncertainties.

2.3 Comparison of EUVE and EOS Filter Tuning Results

The optimum Qdot-to-MNV ratios found for EOS are larger than those found for EUVE solutions by approximately two orders of magnitude. For EUVE, the optimum Qdot-to-MNV ratio ranged from 1.0×10^{-7} to 1.0×10^{-9} when the drag coefficient was not estimated. The corresponding value for the EOS solutions was 5.0×10^{-5}. This is, of course, due to the significantly different conditions under which EOS and EUVE solutions were obtained, especially the different relative error magnitudes of the atmospheric drag and the SST ionospheric refraction uncertainties assumed for the two cases. The EOS solutions were obtained with relatively small SST ionospheric refraction errors and large drag errors, whereas the EUVE solutions were obtained with large SST ionospheric refraction errors and moderate drag errors. This can be seen from Table 4 (EUVE summary) and Table 7 (EOS Series C summary). In addition, the omission of the gravity error contributions and large irregular gaps in the tracking schedule will also cause the optimum Qdot-to-MNV ratios to move toward a smaller value in the case of the EUVE OD scenarios examined here.

2.4 Covariance Analysis Versus Actual Orbit Determination Results

Some actual sequential OD results are available from a recent TONS-EUVE OD analysis report (Reference 1). The solutions presented in that study were obtained using an MNSD value of 0.1 hertz, which corresponds to approximately 0.015 meter/second (in range-rate units). The process noise model used by the TONS sequential OD system is the so-called physically connected process noise model (References 5 and 6), which differs in many respects from the linear growth model used in the present study. The value of 0.1 hertz ($\approx$ 0.015 meter/second) used for MNSD appears to be somewhat high, i.e., one-tenth of this value would be more realistic. However, attempts to use a smaller MNSD value and a proportionately smaller process noise level led to solutions in which good measurements were edited out, probably because such an OD process generates less filter-predicted measurement noise variance, the square-root of which is used for the measurement editing. Therefore, for real OD solutions, it may be acceptable and even desirable to use MNSD values larger than those used in a covariance analysis.

In general, covariance analysis cannot properly address the question of measurement editing. However, an order-of-magnitude estimate of the MNSD value to be used for actual OD solutions may be obtained by computing the prefit root-sum-square (RSS) contributions to the measurement residuals due to all measurement-related error sources. The RMS error of the range-rate measurements due to these error sources may be used for this purpose. For example, in the case of the EUVE OD arc studied here, the ionospheric refraction errors and the TDRS ephemeris errors are the major measurement-related error sources. The RMS values of the measurement errors due to these error sources are found to be 0.011 and 0.0055 meter/second, respectively. These values were obtained after excluding approximately 7 percent of the measurements for which the ionospheric refraction corrections exceeded 0.0505 meter/second. The RSS of these two values and a realistic MNSD value of 0.0014 meter/second give an adjusted MNSD of 0.012 meter/second, which is very close to the MNSD of 0.1 hertz ($\approx$ 0.015 meter/second) used in the actual EUVE OD solutions. The final results for such an MNSD value will depend on other measurement-related error contributions not considered in this example.

A direct application of the results obtained using the ODEAS filter tuning process to the TONS sequential OD solutions is not possible, because in TONS the process noise model used is the physically connected process noise model, which is rather

different from the linear growth model implemented in ODEAS. However, an achievable OD accuracy predicted using the ODEAS model can still be compared to some extent with the corresponding solutions obtained using the TONS model. In the case of EUVE, Group B solutions presented in Table 4 can be used for this purpose. The EUVE total RMS position accuracy achievable is approximately 35 meters (see Group B Case 3 results in Table 4). However, a number of small adjustments are needed for this. First, the random noise contribution has to be adjusted, because the EUVE actual OD solutions were obtained using an MNSD of 0.015 meter/second instead of 0.01 meter/second that was used for the Group B solutions in Table 4. Second, the Group B solutions summarized in Table 4 were obtained with the atmospheric drag error considered, whereas the TONS OD solutions for EUVE were obtained with the drag coefficient solved. Assuming that contributions from other error contributions remain approximately the same when the drag is estimated, the adjusted total RMS error remains approximately the same as 35 meters. As a measure of the TONS-EUVE OD accuracy, Reference 1 reports an RMS total position difference of 30 to 35 meters between the TONS-EUVE OD solutions and the definitive EUVE solutions obtained using the Goddard Trajectory Determination System (GTDS) (Reference 1, Figure 5-3).

The results for EOS PM-1 presented earlier can be similarly adjusted to be applicable to actual OD solutions. It is reasonable to assume that the EOS-TONS OD solutions will be obtained by solving for the drag coefficient and using an MNSD of 0.015 meter/second (0.1 hertz) as was done in the EUVE TONS OD experiment. Then, the results of EOS PM-1 simulation Series D (Table 8) can be used, with adjusted random noise contribution. As discussed earlier, the scale factor for adjustment can be obtained as the ratio of the MNSD values used in actual OD and covariance analysis. This scale factor is computed to be 12.7 (i.e., 0.015/0.00118). The adjusted RMS random noise contributions are 2.42, 20.84, 21.10, and 29.87 meters, respectively, for Cases D1 through D4. Combining these with systematic error contributions, the adjusted total RMS (3σ) positions errors for Cases D1 through D4 are given by 30.58, 29.98, 30.36, and 40.39 meters, respectively. As a result, the first three simulation results are all very close to each other, but simulation D2 remains the optimum case.

3. Summary and Conclusions

A study of filter tuning techniques has been performed using the ODEAS sequential analysis capabilities. The EUVE and EOS results presented in this paper are based on processing 2 days of tracking data. The tracking data distribution for EUVE was taken from the actual EUVE tracking near January 17, 1993; for the EOS tracking data distribution, approximately 20 minutes of tracking per EOS orbit was assumed. In most of the simulation cases, the filter solutions were found to reach steady-state solutions after approximately 1 day of measurement processing. The filter tuning process was based on the ODEAS linear growth model in which the velocity variance growth rate was used to specify the process noise level.

The results demonstrated that the process noise applied for filter tuning can significantly affect the orbit determination errors contributed from various error sources in different ways. It was shown that, in general, the spacecraft position errors contributed from dynamic error sources, such as gravity and atmospheric drag uncertainties, decrease as the process noise level increases. The reverse trend was found to be true for measurement-related error sources, such as satellite-to-satellite ionospheric refraction correction uncertainties, TDRS ephemeris uncertainties, and random noise effects. The choice of optimum filter-tuning parameters, therefore, involves selecting the process noise variance growth rates in such a way that the combined contribution of the dynamic and measurement-related error sources to the OD errors is minimized. It was found that a parameter formed by taking the ratio of the Qdot value to the MNV is convenient for characterizing the statistical properties of the state estimate errors, where Qdot is the velocity variance growth rate used to specify the process noise level. MNV is the square of the MNSD specified for the tracking measurements. This parameter is referred to as the Qdot-to-MNV ratio.

OD solutions obtained using different filter tuning parameters can be characterized in terms of the Qdot-to-MNV ratio and the MNSD value used for each filter tuning simulation case. Characteristic properties of these solutions in terms of the filter tuning parameters are as follows:

- After the filter reaches steady state, state estimate errors due to all systematic (measurement-related and dynamic) error sources are essentially determined by the Qdot-to-MNV ratio only and are independent of the MNSD value used. Steady-state random noise contributions obtained using the same Qdot-to-MNV ratio and different MNSD values are proportional to the MNSD values used.

- Measurement-related error contributions increase and dynamic error contributions decrease as the Qdot-to-MNV ratio increases.

- Magnitudes of the SST ionospheric refraction correction errors and the atmospheric drag-errors were found to play important roles in determing the optimum filter tuning parameters. This means that the larger the magnitudes of the SST ionospheric refraction correction errors, the smaller the optimum Qdot-to-MNV ratio becomes; and the larger the magnitudes of the atmospheric drag-related errors, the larger the optimum ratio becomes.

- An estimated position accuracy of approximately 34 meters can be achieved for EUVE by solving for the drag coefficient, using an MNSD value of 0.015 meter, and setting the Qdot-to-MNV ratio to a value less than 1.0×10^{-9}. When the drag coefficient error is considered, a similar minimum position error can be achieved by using the same MNSD value and a Qdot-to-MNV ratio of 1.0×10^{-8}.

- For the EOS OD scenario, in which the drag coefficient is estimated and an MNSD of 0.015 meters is used, a total position accuracy of approximately 30 meters is achievable using a Qdot-to-MNV ratio of 5.0×10^{-9}. When the drag coefficient error is considered, a position accuracy of approximately 42 meters is achievable using a Qdot-to-MNV ratio of 5.0×10^{-5}.

The optimum Qdot-to-MNV ratio varies with the spacecraft orbital characteristics, tracking scenarios, and estimation parameter set selected. The properties summarized above can be used to reduce the number of simulation cases required for sequential error analysis, as there is no need to vary both Qdot and MNSD values. It is sufficient to generate one series of solutions using different Qdot-to-MNV ratios with a fixed MNSD value. Then, results based on a different MNSD value can easily be obtained from those already available by appropriately scaling the random noise contributions.

References

1. Goddard Space Flight Center, Flight Dynamics Division, 553-FDD-94/001R0UD0, T*racking and Data Relay Satellite System (TDRSS) Onboard Navigation System (TONS) Experiment Final Report*, G. M. Horstkamp et al., prepared by Computer Sciences Corporation, March 1994.

2. A. Gelb et al., *Applied Optimal Estimation*, MIT Press: Cambridge, Massachusetts, 1974.

3. Goddard Space Flight Center, Flight Dynamics Division, 554-FDD-90/029R2UD0, *Orbit Determination Error Analysis System (ODEAS) Mathematical Specifications, Revision 2*, T. Lee and C. Yee (CSC), prepared by Computer Sciences Corporation, September 1993.

4. Stanford Telecommunications, TR93135, *Earth Observing System (EOS) Supplementary Analyses of Navigation Performance Using the TDRSS Onboard Navigation System (TONS)*, M. A. Lorenz et al., September 1993.

5. Goddard Space Flight Center, Flight Dynamics Division, 553-FDD-93/030R1UD0, T*racking and Data Relay Satellite System (TDRSS) Onboard Navigation System (TONS) Flight Software Recommended Algorithms, Revision 1*, A. C. Long et al. (CSC), prepared by Computer Sciences Corporation, December 1993.

6. J. Wright, "Sequential Orbit Determination With Auto-Correlated Gravity Modeling Errors," *Journal of Guidance and Control*, Vol. 4, 1981, p. 304.